# Direct numerical simulation of heterogeneous bubble nucleation

M Saini, S Zaleski, Daniel Fuster

# Direct numerical simulation of heterogeneous bubble nucleation

M. Saini[1,*], S. Zaleski[1] and D. Fuster[1]

[1] Sorbonne Universités, UPMC Univ Paris 06, CNRS, UMR 7190
Institut Jean Le Rond d'Alembert, F-75005 Paris, France

**Abstract**

In this work we numerically simulate the expansion of preexisting bubbles, typically known as heterogeneous nucleation. We use this to predict nucleation thresholds for single bubble attached to walls and study the dependency of this threshold on the solid surface properties. To that end we modify the boundary conditions at the wall to demonstrate the critical effect of two limiting boundary conditions to correctly predict the nucleation threshold of bubbles: a) The contact point is receding freely at a constant angle of contact b) The contact point is pinned at particular location and cannot move due to obstruction. The understanding of heterogeneous bubble nucleation is very important to devise techniques of well controlled cavitation for biomedical applications such as histotripsy, lithotripsy etc.

**Keywords:** Bubbles, Nucleation, Cavitation, CFD, all-Mach.

## 1 Introduction

Bubble nucleation is an important aspect of cavitation and an integral part of understanding dynamics of cavitation. Generally in heterogeneous nucleation, the bubbles appear randomly biased to different locations on solid boundaries, from where these bubbles with different initial sizes grow unstably by several orders of magnitude under certain favorable conditions [1, 2]. The unified perspective of heterogeneous nucleation given by Atchley and Prosperetti [3] combining the idea of unstable growth with the crevice model to predict the threshold for heterogeneous nucleation. Brokent et. al. [4] predicted these thresholds experimentally but the literature is devoid of any CFD studies of heterogeneous bubble nucleation.

In the current study we simulate numerically the process of bubble nucleation after a sudden pressure decrease. In Section 2, we discuss briefly the proposed numerical method to simulate process of heterogeneous bubble nucleation and also setup of the problem. We find the thresholds based on already existing theories discussed in Section 3. We also recognise the effect of boundary condition at wall on the process of heterogeneous nucleation and thresholds for heterogeneous nucleation. In Section 4, we discuss the results for numerical prediction of nucleation threshold and compare with theories, we also numerically verify the of effect of boundary conditions on process of nucleation. We conclude the current study in Section 5.

## 2 Numerical setup and problem description

### 2.1 Numerical solver

The basilisk [5] software is chosen for current study and in particular we use the all-mach solver proposed by Fuster and Popinet [6] that we present here in brief. The interface between the two fluids is represented by a geometric volume of fluid (VOF) method. The six equation model is used in which the primitive variables are mass per unit volume ($\rho$), momentum per unit volume ($\rho\mathbf{u}$), total energy per unit volume (sum of internal and kinetic energy $\rho e + 1/2\rho\mathbf{u}^2$). The velocities are assumed to be in equilibrium at

*Corresponding author, Mandeep Saini: mandeep.saini@sorbonne-universite.fr

the interface. The jump in other quantities is diffused over length of one grid cell. The averaged values based on color function are stored in the interfacial cells which is well known as one fluid approach. The conservation equations for primitive variables are solved using finite volume method. These equations are as follows

$$\frac{\partial \rho_i}{\partial t} + \nabla \cdot (\rho_i \mathbf{u}) = 0 \tag{1}$$

$$\frac{\partial \overline{\rho}\mathbf{u}}{\partial t} + \nabla \cdot (\overline{\rho}\mathbf{u}\mathbf{u}) = -\nabla p + \nabla \cdot \tau^{'} + \sigma\kappa\nabla c_i \tag{2}$$

$$\frac{\partial(\rho_i e_i + 1/2\rho_i \mathbf{u}_i^2)}{\partial t} + \nabla \cdot (\rho_i e_i \mathbf{u} + 1/2\rho_i \mathbf{u}_i^2 \mathbf{u}) = -\nabla \cdot (\mathbf{u}p) + \nabla \cdot (\tau_i^{'}\mathbf{u}) + \sigma\kappa\nabla c_i \mathbf{u} \tag{3}$$

The subscript $i$ in above equations represent $i_{th}$ phase. The viscous stress tensor is given as $\tau^{'} = \mu(\nabla\mathbf{u} + (\nabla\mathbf{u})^T)$, p is pressure, $c_i$ is volume fraction of $i_{th}$ phase, sigma is surface tension force between two fluids and $\kappa$ is curvature. The advection equation is solved for color function which is typical in VOF. It represent that the interface is evolving with local flow velocity. The equation for color function is given as

$$\frac{\partial c_i}{\partial t} + \mathbf{u} \cdot \nabla c_i = 0 \tag{4}$$

The classical projection method of incompressible flow solvers is used to solve the above equations. In the advection step the left hand side of eqs. 1 - 3 is solved along with the advection equation of VOF to have a consistent formulation. After advection step the provisional values of primitive variables is obtained. Then, the full momentum equation is solved using gradient of pressure at previous time step which is then removed to get another provisional values of momentum. The source term due to surface tension is added as a volumetric force as typically done in continuum surface force models. In next step, the pressure is predicted from evolution equation (Helm-Holtz equation) to calculate fluxes for momentum and energy. Eventually at end of time step the pressure is predicted from EOS. The well known stiffened gas EOS is used in the formulation which is given as

$$\rho_i e_i = \frac{p_i + \Gamma_i \Pi_i}{\Gamma_i - 1} \tag{5}$$

We extend the method to include the contact angle implementation strategies for height functions given by Afkami and Bussman [7]. The combination of two is proposed as comprehensive methodology for numerically simulating the process of nucleation of bubble attached to wall. Such that the bubble is assumed to be receding at constant angle of contact. We also implement pinning boundary condition by putting zero velocities and homogeneous Neumann pressure gradients in cells next to wall. The detailed discussion on importance of wall boundary conditions on bubble nucleation at walls is discussed in upcoming sections.

## 2.2 Problem description

The numerical setup for simulation of heterogeneous bubble nucleation is shown in Figure 1. The domain is square whose size is 100 times the initial contact length of bubble. The bottom boundary is considered as axis of symmetry, left boundary is considered as slip wall, right and top boundaries are considered as outflow boundaries. As typical in VOF methods, interface is defined by piece wise linear approximation of spherical cap in the bottom left corner of the domain. The volume inside is initialised with gas properties and outside with liquid. The initial gas pressure is represented as $p_{g,0}$. The bubble is assumed to be in equilibrium such that liquid pressure just outside the bubble ($p_0$) is given by Young-Laplace equation $p_0 = p_{g,0} - 2\sigma/R_{c,0}$. The liquid pressure far from bubble ($p_\infty$) is less than that close to bubble by amount $\Delta p$. Consistent with Rayleigh Plasset type models, the initial pressure in liquid is assumed to drop with inverse of radial distance (r) from bubble center i.e. $p(r,0) = p_\infty - (p_0 - p_\infty)R_{c,0}/r$, where $R_{c,0}$ is initial radius of curvature of the bubble.

Other relevant dimensionless numbers important for the problem are given in Table 1. The liquid is assumed to be the reference phase and all dimensionless numbers are defined on basis of liquid properties (represented by subscript '$l$'). The density and viscosity contrast for liquid and gas are assumed to be that close to water-air i.e. $\rho_l/\rho_g = 1000$ and $\mu_l/\mu_g = 100$.

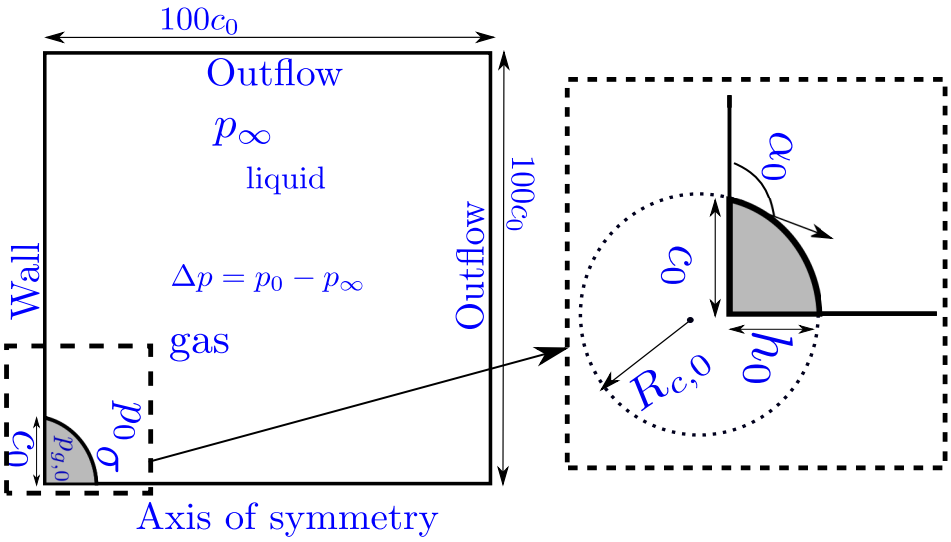


Figure 1: Left: The numerical setup and boundary conditions for simulations of heterogeneous bubble nucleation. Right: The geometrical parameters commonly used to describe the shape character of a spherical cap.

| Weber (We) | Reynolds (Re) | Mach (Ma) |
|---|---|---|
| $\frac{p_0 R_{c,0}}{\sigma}$ | $\frac{\sqrt{\Delta p \rho_l} R_{c,0}}{\mu_l}$ | $\sqrt{\frac{\Delta p}{\rho_l c_l^2}}$ |

Table 1: Definition of dimensionless numbers relevant for simulations of heterogeneous nucleation

## 3 Theory of heterogeneous bubble nucleation

The theory of bubble nucleation was first discussed formally in letters of Harvey [8] where he represented the surface defects as a triangular pit. Then, there are various studies that discuss the movement of gas liquid interface in pits [9, 1]. The unified prospective was provided by Atchley and Prosperetti [3]. They show that unstable growth is important ingredient to predict threshold for nucleation of bubbles which is missing in previous studies. The experimental verification of this model is presented recently by Brokent et. al. [4]. Fuster et. al. [10] provide an alternative approach based on system free energy to predict similar conditions for unstable growth.

The idea of unstable growth was first observed by Blake [11] for spherical bubbles. The spherical bubble in bulk of infinite liquid becomes unstable and grows by several orders of magnitude, if they expand to a critical radius called Blake's radius. The Laplace pressure corresponding to this radius reaches minimum and called the Blake's threshold. For non-spherical bubbles emerging from sub-micron sized surface defects, the Laplace pressure depends on geometrical description of the bubble. If we assume, that the bubble is a spherical cap, and surface is perfectly flat (No crevice/pits), the complete geometrical description is provided by two parameters. The four most common parameters to represent spherical caps are the radius of curvature ($R_c$), the angle of contact ($\alpha$), the vertical height of of cap (h) and the length of contact at the bottom (c). These are represented for an initial configuration in Figure 1 on right, where the subscript '0' signifies their values for initial stable configuration. In terms of c and h the Laplace pressure for a quasi-statically expanding spherical cap shaped gas bubble in absence of of heat and mass transfer can be written as following

$$\frac{p_l}{p_0} = \left(1 + \frac{2}{We}\right)\left(\frac{3h_0c_0^2 + h_0^3}{3hc^2 + h^3}\right)^\gamma - \frac{2}{We}\frac{h_0^2 + c_0^2}{h^2 + c^2}\frac{h}{h_0} \tag{6}$$

Where we define Weber number as $We = p_0 R_{c,0}/\sigma$. The evolution of c and h depends on bubble behavior and dynamics of motion of contact line at the wall. The complete description of contact point motion at the wall is extremely complicated physics problem due to disagreement of moving contact line with the no slip boundary condition at wall, moreover all surfaces are generally heterogeneous which poses contact angle different the static value [12]. In current study, we choose two limiting cases:

1. A contact line slowly receding at a constant angle of contact ($\alpha = \alpha_0$)
2. A pinned contact line ($c = c_0$)

Imposing these conditions on Equation 6 the problem of finding nucleation threshold is reduced to a single variable minimization problem which we solve numerically. The results plotted in Figure 2 represent the critical value of pressure drop $\Delta p_c/p_0$ for a given bubble represented by $(c_0, h_0)$ at a reference ambient pressure $p_0$ and surface tension $\sigma$. Typically $p_0 \approx \mathcal{O}(10^5)$ and $\sigma \approx \mathcal{O}(10^{-2})$ thus we plot stability curves of bubbles for which c & h are of $\mathcal{O}(100nm)$. For reference we include the critical region for a pressure drop equal to 20 times initial ambient pressure shown by thick black curves. All bubbles lying inside the isobar represented by thick black line (i.e. bottom left corner) are stable and all bubbles which are outside this (i.e. top right part of the diagram) are unstable and grow. Comparing two figures, we can see that very small bubbles are stable and large bubbles are unstable. Remarkably, there is an intermediate regime where bubbles can behave stably or unstably depending upon the condition imposed on the movement of the bubble. This effect is discussed in detail in Section 4.

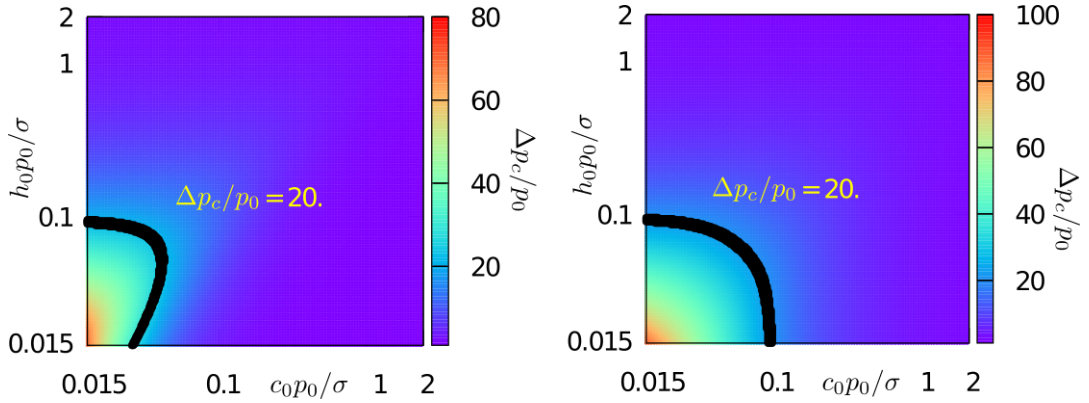


Figure 2: The predictions of critical pressure drop for different bubble sizes when Left: bubbles evolve under the condition of constant angle of contact at wall, Right: bubble evolves with constant length of contact at the wall

# 4 Results and discussion

## 4.1 Numerical prediction of the nucleation threshold

| Weber (We) | Reynolds (Re) | Mach (Ma) |
|---|---|---|
| 1 | $\infty$ | 0.05 |

Table 2: The dimensionless parameters for predicting thresholds of bubbles attached to wall

We start by predicting thresholds for unstable growth of bubbles attached to wall. The dimensionless parameters are shown in Table 2. We impose that the angle is known and remain constant throughout the simulation. We vary $\Delta p$ with respect to the $\Delta p_c$ predicted with the static theory presented in section 3. The temporal evolution of the dimensionless bubble volume $(V/V_0)^{1/3}$ is plotted in Figure 3 left. The bubble shows unstable growth for $\Delta p \approx 0.97\Delta p_c$. The critical threshold is under predicted by DNS as compared with the static theory because liquid inertia alters the behaviour of bubble specially close to critical point by expanding beyond the critical size, which in the limit of a spherical bubble corresponds to the Blake's radius.

Atchley and Prosperetti [3] show that for bubble motion outside the crevice, if bubble crevice volume ¡¡ bubble volume and it is assumed to expand with constant contact angle ($\alpha_{t=t} = \alpha_{t=0}$), the nucleation threshold is independent of angle of contact and is function of Radius of curvature only (Similar to spherical bubble). In Figure 3 on right, the solid black line is isobar for $\Delta p_c/p_0 = 1.86$ which coincides with constant radius of curvature line represented by red points. For all these points condition for unstable growth predicted numerically is $(\Delta p/p_0)_{num} = 1.8$. Thus we predict the threshold by DNS which is under-predicted by 3.22 % compared to static theory owing to dynamic effects.

## 4.2 Effect of boundary conditions

| $\Delta p/p_0$ | Weber (We) | Reynolds (Re) | Mach (Ma) |
|---|---|---|---|
| 1.86 | 1.41 | 10 | 0.05 |

Table 3: The dimensionless parameters for predicting thresholds of bubbles attached to wall

The left curve in Figure 4 is obtained by plotting the isobars obtained in Section 3 for $\Delta p_c/p_0 = 1.86$ on same $c_0$ vs $h_0$ plane for both constant angle of contact ($\alpha = \alpha_0$) and constant length of contact ($c = c_0$). The following three regions can be identified

Region I: Bubbles are stable irrespective of the behavior of the contact line.

Region II: The stability of the bubble depends on how the contact line moves at the wall and thus numerically its response is sensitive to the boundary condition imposed at the wall.

Region III: Bubbles are always unstable and grow several orders of magnitude irrespective of the response of the contact line.

To demonstrate this effect numerically we choose the representative bubble size $c_0p_0/\sigma = 1.25$,$h_0p_0/\sigma = 0.75$, i.e. circular red dot in Figure 4, which lies in the region II. The parameters for the problem are given in Table 3. We run simulations successively for the following boundary conditions a) constant contact angle and free slip condition for velocity b) The no slip BC for velocity and interface in pinned by putting zero velocities in cells next to wall also the pressure in these cells is extrapolated form inside of domain i.e. $\partial p/\partial x = \partial p/\partial y = 0$. None of the boundary conditions accurately represent the physics of moving contact lines, nevertheless these tests give us the fair idea about the influence of wall boundary condition on the threshold of bubble nucleation and stability of bubbles. The evolution of representative bubble subjected to different wall conditions in successive numerical experiments is shown in Figure 4 on right. In line with the the curve based on Section 3 the bubble is shows stable oscillations about new mean radius when subjected to constant contact length boundary condition whereas grow unstably when subjected to constant contact angle boundary condition.

We also plot the numerical as well as theoretical predictions of Laplace pressure against the volume and the bubble shapes at various instants of time. The Laplace pressure reaches the minima (corresponding critical volume) in the case of $\alpha = \alpha_0$ where as the minima is not reached in the case of $c = c_0$ thus former is unstable and latter is stable.

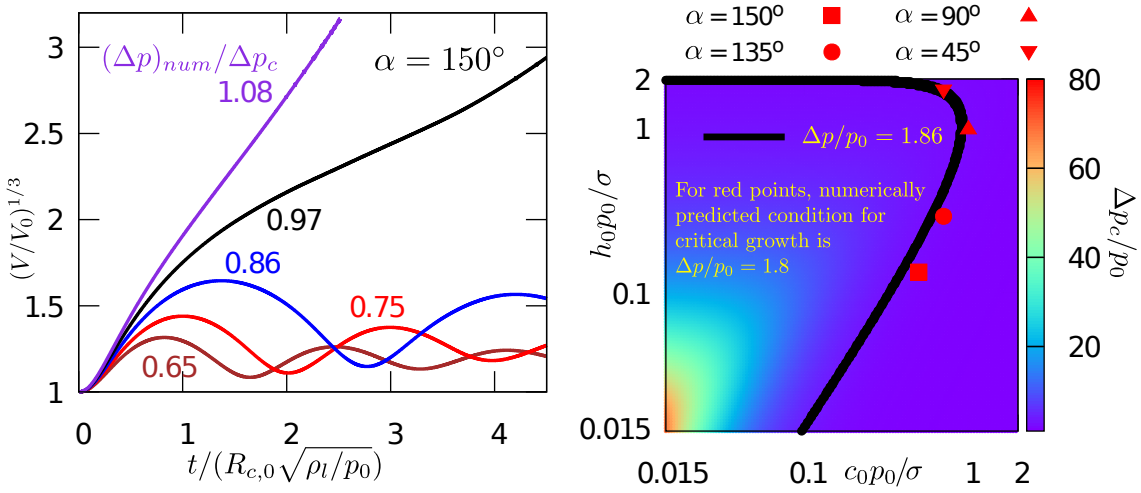


Figure 3: Left: The evolution of dimensionless bubble volume evolution for bubble that evolves with constant contact angle $\alpha = 150°$ for different pressure drops compared with the critical pressure drop predicted from static theory. For this problem Re $= \infty$ and We $= 1$. Right: The color-map is variation of critical $\Delta p$ predicted in Section 3. Solid black line is isobar corresponding to $\Delta p_c/p_0 = 1.86$ which coincides with red colored (constant initial radius of curvatures $R_{c,0} = 1$) points and for all these points the numerically predicted values i.e. $(\Delta p_c)_{num}$ is 1.8. Thus it also shows the comparison between the theory and DNS.

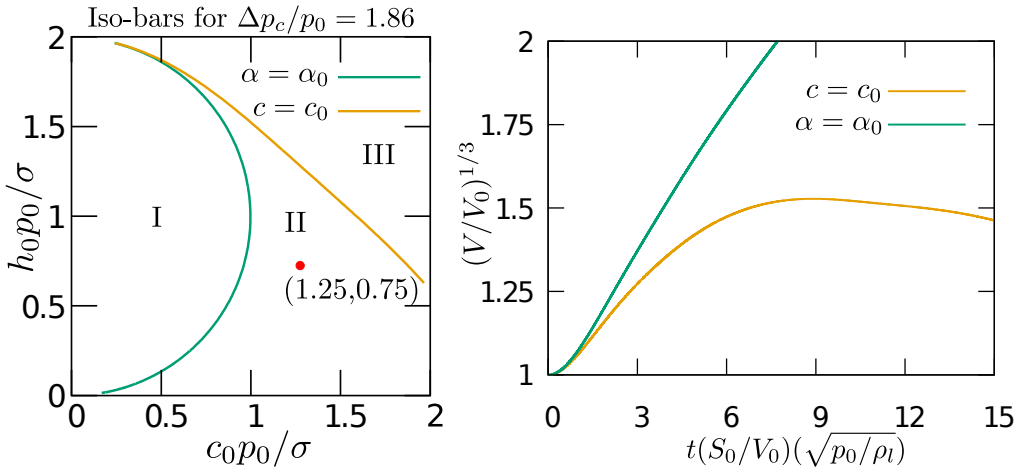


Figure 4: Left: Stability curve for bubble sizes subjected to pressure drop of 1.86 times the initial ambient pressure and subjected to different behaviour of contact point at wall: constant angle of contact ($\alpha = \alpha_0$) and constant length of contact ($c = c_0$). The red point is chosen as representative of intermediate region where the stability of bubble is dependent on the behaviour of contact line. Right: The evolution of bubble volume obtained from DNS for the same bubble (represented by red point in figure on left) under same pressure drop subject to two different boundary conditions $\alpha = \alpha_0$ and $c = c_0$

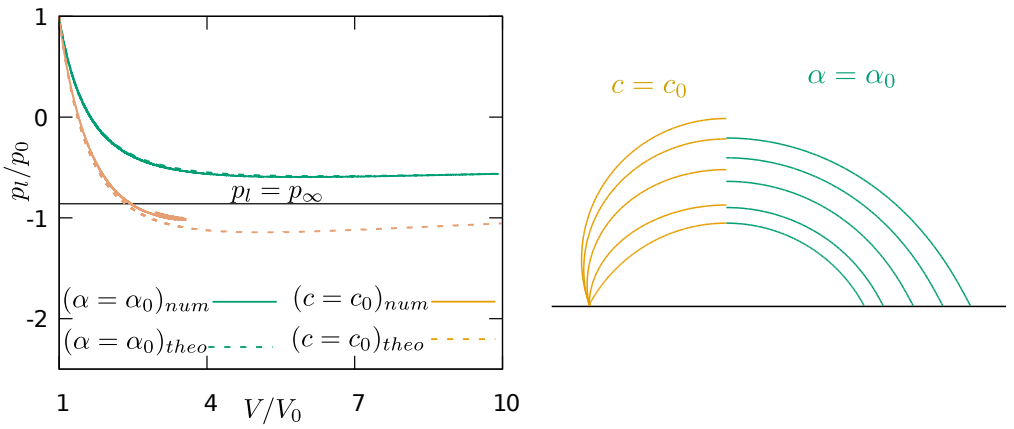


Figure 5: Left: Numerically calculated Laplace pressure compared with theoretical estimates of Section 3 for two boundary conditions i.e. constant angle of contact ($\alpha = \alpha_0$) and constant length of contact ($c = c_0$) The theoretical estimates are plotted with dotted lines and results of DNS with solid lines, Right: The interface at various instances of time for same boundary conditions of $\alpha = \alpha_0$ and $c = c_0$

## 5 Conclusions

A new method for simulations of heterogeneous bubble nucleation is proposed. The numerical predictions of threshold for bubble nucleation are obtained. The numerical predictions are in good agreement with the ones predicted from static theory. The thresholds are slightly under predicted owing to inertial effects which were neglected in the static stability analysis. It is shown that, theoretically, the threshold for nucleation depends on the behaviour of triple point of contact at wall. The limiting case of evolution at boundary i.e. constant angle of contact and constant length of contact (pinning) are analysed. Three regions are identified for a given pressure drop, in which bubbles are definitely stable, definitely unstable or stable/unstable depending on boundary conditions. The same is also verified numerically by using the method proposed for simulating the process of bubble nucleation. Although we did not account for the motion of contact line accurately but we get fair idea of existence of intermediate region of bubble sizes for which surface properties can play important role for estimating nucleation thresholds.

**Acknowledgments:** This work is supported by European Union (EU) under MSCA-ITN program called Ultrasound Cavitation in sOft Matters (UCOM).

# References

[1] Robert E Apfel. The role of impurities in cavitation-threshold determination. *The Journal of the Acoustical Society of America*, 48(5B):1179–1186, 1970.

[2] Lawrence A Crum. Tensile strength of water. *Nature*, 278(5700):148–149, 1979.

[3] Anthony A Atchley and Andrea Prosperetti. The crevice model of bubble nucleation. *The Journal of the Acoustical Society of America*, 86(3):1065–1084, 1989.

[4] Bram M Borkent, Stephan Gekle, Andrea Prosperetti, and Detlef Lohse. Nucleation threshold and deactivation mechanisms of nanoscopic cavitation nuclei. *Physics of fluids*, 21(10):102003, 2009.

[5] Stephane Popinet. Basilisk. *URl: http://basilisk. fr.(accessed: 10.21. 2019)*, 2014.

[6] Daniel Fuster and Stéphane Popinet. An all-mach method for the simulation of bubble dynamics problems in the presence of surface tension. *Journal of Computational Physics*, 374:752–768, 2018.

[7] S Afkhami and M Bussmann. Height functions for applying contact angles to 2d vof simulations. *International journal for numerical methods in fluids*, 57(4):453–472, 2008.

[8] E Newton Harvey. Decompression sickness and bubble formation in blood and tissue, bull. *Anesthesiology: The Journal of the American Society of Anesthesiologists*, 7(4):457–457, 1946.

[9] M Strasberg. Onset of ultrasonic cavitation in tap water. *The Journal of the Acoustical Society of America*, 31(2):163–176, 1959.

[10] Daniel Fuster, Kim Pham, and Stéphane Zaleski. Stability of bubbly liquids and its connection to the process of cavitation inception. *Physics of Fluids*, 26(4):042002, 2014.

[11] EA Neppiras and BE Noltingk. Cavitation produced by ultrasonics: theoretical conditions for the onset of cavitation. *Proceedings of the Physical Society. Section B*, 64(12):1032, 1951.

[12] Terence D Blake. The physics of moving wetting lines. *Journal of colloid and interface science*, 299(1):1–13, 2006.